PTEP

Prog. Theor. Exp. Phys. **2015**, 043F01 (14 pages)
DOI: 10.1093/ptep/ptv041

Direction-sensitive dark matter search with gaseous tracking detector NEWAGE-0.3b'

Kiseki Nakamura[1,*], Kentaro Miuchi[2], Toru Tanimori[1], Hidetoshi Kubo[1], Atsushi Takada[1], Joseph D. Parker[1], Tetsuya Mizumoto[1], Yoshitaka Mizumura[1], Hironobu Nishimura[1], Hiroyuki Sekiya[3], Atsushi Takeda[3], Tatsuya Sawano[1], Yoshihiro Matsuoka[1], Shotaro Komura[1], Yushiro Yamaguchi[2] and Takashi Hashimoto[2]

[1]*Department of Physics, Kyoto University, Oiwakecho, Sakyo-ku Kyoto-shi, Kyoto, 606-8502, Japan*
[2]*Department of Physics, Kobe University, Rokodai, Nada-ku Kobe-shi, Hyogo, 657-8501, Japan*
[3]*Kamioka Observatory, ICRR, The University of Tokyo, Gifu, 506-1205 Japan*
[*]E-mail: nakamura@cr.scphys.kyoto-u.ac.jp

Received August 21, 2014; Revised February 27, 2015; Accepted February 27, 2015; Published April 15, 2015

NEWAGE is a direction-sensitive dark matter search experiment using a micro-time-projection chamber filled with CF_4 gas. Following our first underground measurement at Kamioka in 2008, we developed a new detector with improved sensitivity, NEWAGE-0.3b'. NEWAGE-0.3b' has twice the target volume of the previous detector, a lower energy threshold, and an improved data acquisition system. In 2013, a dark matter search was undertaken by NEWAGE-0.3b' in Kamioka underground laboratory. The exposure of 0.327 kg · days achieved a new 90% confidence level direction-sensitive spin-dependent cross-section limit of 557 pb for a 200 GeV/c^2 weakly interacting massive particle. Relative to our first underground measurements, the new direction-sensitive limits are improved by a factor of ∼10, and are the best achieved to date.

Subject Index F41

1. Introduction

Numerous observations of the universe suggest that a large fraction of the Universe's mass is comprised of non-baryonic dark matter [1]. The weakly interacting massive particle (WIMP) is one of the leading candidates for the dark matter [2]. WIMPs within the halo of our galaxy are expected to be detected on Earth; in particular, the signals of WIMP-nucleus elastic scatterings should be detectable in direct search experiments [3]. The energy spectrum of WIMP signals is expected to be similar to an exponential distribution, and the relevant energy region is considered to be below 100 keV. The low expected event rate is attributable to the small cross-section of the interaction between WIMPs and ordinary matter. Therefore, WIMP detection experiments must be performed in low-background environments, and are thus typically undertaken in underground facilities.

Many direct search experiments for dark matter have been performed to date. Although observations of the annual modulations of event rates have yielded positive results, none of these results has been universally accepted. Therefore, to obtain more robust evidence of dark matter, another distinct signal detectable by a direction-sensitive method should be searched for. Since the Cygnus constellation is viewed in the forward direction of the Solar system's motion, dark matter would seem to arrive from the Cygnus direction as a "WIMP-wind." The forward and backward scattering recoil angles, relative to the expected wind direction, should exhibit a large asymmetry (>10 times

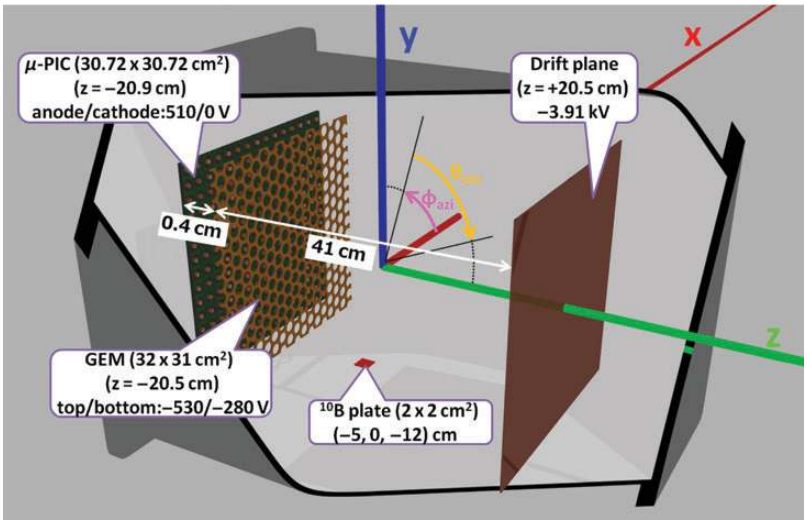

Fig. 1. Schematic of NEWAGE-0.3b'. The coordinate system with origin at the center of the detection volume is also shown. Red, blue, and green lines indicate the x, y, and z axes, respectively. Energy is calibrated by a glass plate coated with a thin layer of ^{10}B at $(-5, 0, -12)$.

in the typical energy range) [4]. Since the direction of Cygnus relative to Earth varies both daily and annually, the systematic error introduced by the daily and seasonal environmental variation will be reduced. A low-pressure gaseous detector with high positional resolution is suitable for detecting tracks shorter than 1 mm in atmospheric pressure gas. The NEWAGE experiment searches for distinct dark matter signals generated in low-pressure gaseous time-projection chambers (TPCs).

2. Detector

The sensitivity of our previous measurements, performed by NEWAGE-0.3a [5], has been enhanced tenfold by our improved direction-sensitive dark matter detector, NEWAGE-0.3b'. NEWAGE-0.3b' consists of a μ-TPC, its electronics system, and a gas circulation system with cooled charcoal. NEWAGE-0.3b' has twice the target volume of NEWAGE-0.3a, a lower energy threshold, and an improved data acquisition system. Since NEWAGE-0.3b' is operationally similar to NEWAGE-0.3a [5], we summarize the essential properties here, and detail the new properties.

2.1. System

A schematic of the μ-TPC and its inner structure is shown in Fig. 1. The μ-TPC consists of a two-dimensional fine-pitch imaging device known as a micro-pixel chamber (μ-PIC) [6], a gas electron multiplier (GEM) [7], and a detection volume ($30 \times 30 \times 41$ cm^3) filled with CF_4 gas at 0.1 atm. The x, y, and z axes are defined in Fig. 1. The length unit adopted in this paper is cm, unless otherwise stated. Being an imaging detector, the μ-PIC works as the main gas-amplifier and also as the readout electrodes. The area of the μ-PIC is 30.72×30.72 cm^2, corresponding to 768×768 pixels with a pitch of 400 μm, connected by 768 anode strips and 768 cathode strips. Since the anode and cathode strips are orthogonally configured, we can obtain the two-dimensional position of a hit pixel. To ensure sufficient gas gain, a GEM is placed 4 mm above the μ-PIC as a sub-amplifier. The effective area of the GEM (31×32 cm^2) covers the whole area of the μ-PIC. To reduce discharge damages, the GEM area is segmented into eight sub-areas. The GEM is built onto a 100 μm-thick liquid crystal polymer, and the hole size and pitch are 70 μm and 140 μm, respectively. The drift length, determined

by optimizing the tradeoff between the target-increase advantage and the deterioration of the angular resolution caused by a long drift path, is 41 cm. The electric field is formed by the drift plane and 1 cm-spaced wires on the side walls of the drift region. Polyetheretherketone (PEEK) was newly adopted as the material for the side walls in the NEWAGE-0.3b' detector because the glass-reinforced fluoroplastic used in the NEWAGE-0.3a walls emanated significant amounts of radon. The voltages applied to the μ-PIC, GEM, and the drift plane are stated in Fig. 1. These voltages realized stable operation with a combined (μ-PIC$\times$GEM) gas gain of 2500. For energy calibration purposes, a glass plate coated with a thin layer of ^{10}B was installed at $(-5, -12, 0)$ cm. The μ-TPC was placed in a 2.5 cm-thick stainless steel vacuum vessel filled with CF_4 gas at 0.1 atm. Since the diffusion of a drifting electron is small in CF_4 gas and fluorine has a large spin-dependent (SD) WIMP-proton cross-section, CF_4 gas is a suitable choice for direction-sensitive SD dark matter searching.

NEWAGE-0.3b' was supplemented with a gas circulation system using cooled charcoal. This system was developed to reduce radon, a serious background in dark matter searches, and to maintain the quality of the gas (gas gain and drift velocity) over long-term operation (exceeding one month). The gas in the vessel was continuously circulated by an oil-free pump (XDS5 Scroll Pump [EDWARDS]) and was pushed through 100 g of charcoal (TSURUMICOAL 2GS), which absorbed the radon and other impurities. The flow rate was controlled at 500 ml min^{-1} by a needle-like valve. Stable cooling at 230 K was realized by controlling a heater, while the cooler (CT-910 Cool Man Trap [SIBATA]) was always operated at its maximum cooling power. With this circulation system, the radon rate at 20 days from gas change was reduced by $1/50$ compared to the rate without the system.

A data acquisition system (DAQ) with electronics dedicated to the μ-PIC readout was adopted for the NEWAGE-0.3b' detector [8]. The DAQ system records two data types: "charge" and "track." The "charge" data are recorded by amplifying the analog signals from the 768 cathodes and grouping them into four channels. The waveforms from the four channels are then recorded by a 100 MHz flash ADC. The summed waveforms (FADC-sum) are used to calculate the energy deposition of a charged particle. The "track" data record the addresses and time-over-threshold (TOT) of all strips hit by an event. The TOT is measured as the clock duration between rising and falling edges crossing the threshold, which roughly corresponds to the deposited energy. Since the drift velocity is 8 cm ms^{-1}, 1 clock corresponds to 0.8 mm. Figure 2 shows an example of a track. This newly adopted data acquisition mode, called "DAQ-mode5," measures the TOT by updating the electronics firmware. Additional information of the energy deposition on each strip is provided by the energy loss of the charged particles. The previous mode "DAQ-mode1" reduces the size of the recorded data by noting the x–y coincidences and limiting the number of output addresses. The differences between the two DAQ modes are summarized in Table 1.

2.2. *Energy calibration*

Energy is calibrated using α particles rather than γ-rays and β-rays, since we are interested in the detector response to nuclear tracks, which are expected to result from WIMP-nucleus scatterings. The α particles were generated by neutron capture of ^{10}B in the $^{10}\mathrm{B}(n, \alpha)^7\mathrm{Li}$ reactions ($Q = 2.310$ or 2.792 MeV). α particles are generated in the μ-TPC by irradiating the ^{10}B plate in the μ-TPC (see Fig. 1) with thermalized neutrons. In order to irradiate the thermal neutrons from outside for calibration, we placed a ^{252}Cf neutron source surrounded by polyethylene outside of the detector. This neutron-capture reaction usually emits prompt gamma rays, thus the kinetic energy of the generated α particle is 1.5 MeV. The linearity of the TPC response has been evaluated from the α particles in

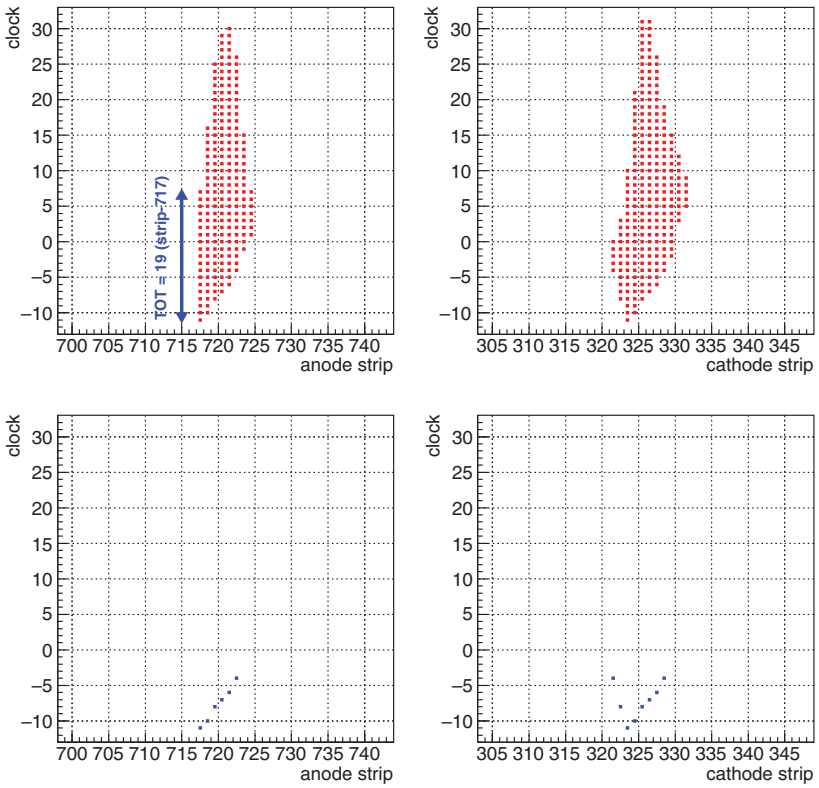

Fig. 2. Example of "raw track data" of an alpha particle. The measured energy was 600 keV. The points shown are of recorded digital hits in the clock anode (z–x) and clock cathode (z–y) strips. Upper figures show real data obtained with DAQ-mode5; lower figures show the emulated DAQ-mode1 data for the same event. In the upper figures, vertical length indicates the TOT of each strip.

Table 1. Difference between DAQ modes 1 and 5.

DAQ mode	mode1	mode5
x–y coincidence	take	not take
strip address to record at each clock	$X_{\min}$, $X_{\max}$, $Y_{\min}$, $Y_{\max}$	all
Time over threshold (TOT)	not take	take
detector	NEWAGE-0.3a	NEWAGE-0.3b'

the background radon. Both ^{220}Rn and ^{222}Rn and their progenies make a peak at $\sim$6 MeV but have a difference of about 10%. Since the detector is not able to measure the ratio of these two types of radon, we regarded the linearity of 6 MeV as 10%.

The energy resolution consists of two factors: non-uniformity of the detector response ($\sigma_{\rm uni}$) and electronic noise ($\sigma_{\rm noise}$). The former is sourced from the positional dependence of the gas gain and the disappearance of electrons drifting in the gas volume. This factor is energy independent and was evaluated from the width of the radon peak as $\sigma_{\rm uni} = 20\% \pm 5\%$. The latter was evaluated from the flash ADC data. Given that the off-timing waveforms and on-timing data are processed in the same manner, the electronic noise was evaluated as $\sigma_{\rm noise} = 2$ keV in 50 keV.

2.3. Event selection

To reduce the background, several event selections are applied. During the dark matter analysis, a fiducial cutting volume of $28 \times 24 \times 41\,{\rm cm}^3$ was selected from the detection volume of

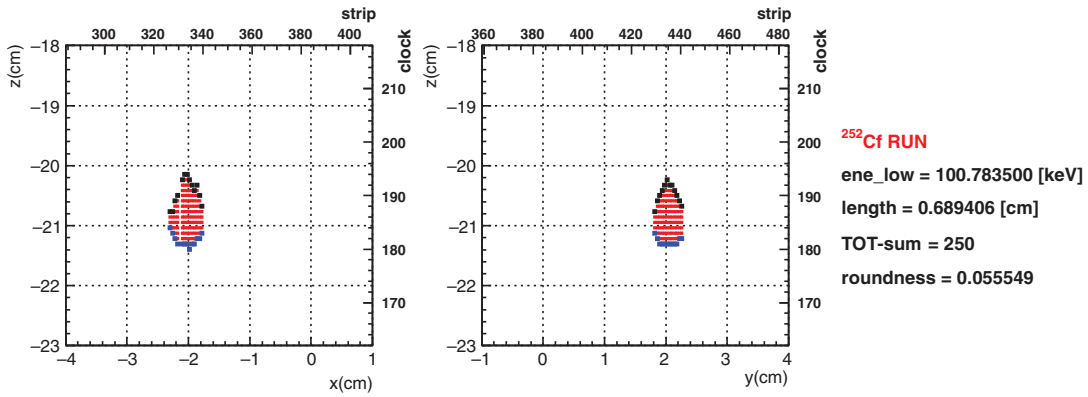

Fig. 3. Track sample measured with a ^{252}Cf source. The left and right panels show the z–x and z–y projections, respectively, of the digitized track. The rise-time points, fall-time points, and the in-between points are indicated in blue, black, and red, respectively. The illustrated event has survived the length cut, the TOT-sum cut, and the roundness cut.

$30.72 \times 30.72 \times 41\,\mathrm{cm}^3$. This procedure rejected charged particles ejected from the walls and the ^{10}B plate. Fiducial cutting was applied to all measurements except the ^{10}B calibration.

The gamma-ray background and the alpha-ray background are then cut by the following criteria. Since the energy loss (dE/dx) of an electron is much smaller than that of a nucleus, the track of electron events should be long (Fig.4) and non-continuous (Fig. 5) compared to the track of nuclear events (Fig. 3). The differences in track length and energy-loss density between these particle species were quantified by two parameters: "length" and "TOT-sum." The parameter "length" is calculated as follows. In the x–z and y–z planes, rising points are fitted by straight lines. Here, the rising points have information about the track shape whereas time durations correspond to the energy deposition. Then, the range of rising points along the fitted line is calculated on each plane. After that, the "length" in the 3D space is calculated. The other parameter, "TOT-sum," is the sum of the TOTs of all strips. The TOT of a given strip is the length between the blue (rise time) and black (fall time) points along the strip. Thus, the TOT-sum of a single event is the total number of blue, red, and black points, where the red points lie between the start and end points of the event. Also, since the drift length of the alpha-ray background from radioactive impurities contaminating the μ-PIC is short, gas diffusion is small, and the track shape is close to a straight line (Fig. 6). In order to discriminate this alpha-ray background by using track shape, a "roundness" parameter is defined by Eqn. (1) as the extent to which the shape of the rise points deviates from a straight line.

$$\mathrm{roundness_x} = \frac{\sum^{N_\mathrm{x}} (z_\mathrm{risex} - a_\mathrm{x} x - b_\mathrm{x})^2}{N_\mathrm{x}}, \quad \mathrm{roundness_y} = \frac{\sum^{N_\mathrm{y}} (z_\mathrm{risey} - a_\mathrm{y} y - b_\mathrm{y})^2}{N_\mathrm{y}},$$
$$\mathrm{roundness} = \min(\mathrm{roundness_x}, \mathrm{roundness_y}), \tag{1}$$

where N_x and N_y are the number of hits on the x and y strips, respectively. z_risex and z_risey are the minimum z values, corresponding to the blue points in Figs. 3–6, and (a_x, b_x) and (a_y, b_y) are the best-fit straight lines obtained by fitting (x, z_risex) and (y, z_risey), respectively.

The dependences of the length, TOT-sum, and roundness of nuclear tracks generated by ^{252}Cf and electron tracks generated by ^{137}Cs are shown in Figs. 7–9. Based on these figures, we determined three cut parameters for discriminating between nuclear and electron events:

- **length cut**: track length [cm] $> 0.6 + 0.004 \times$ E [keV].

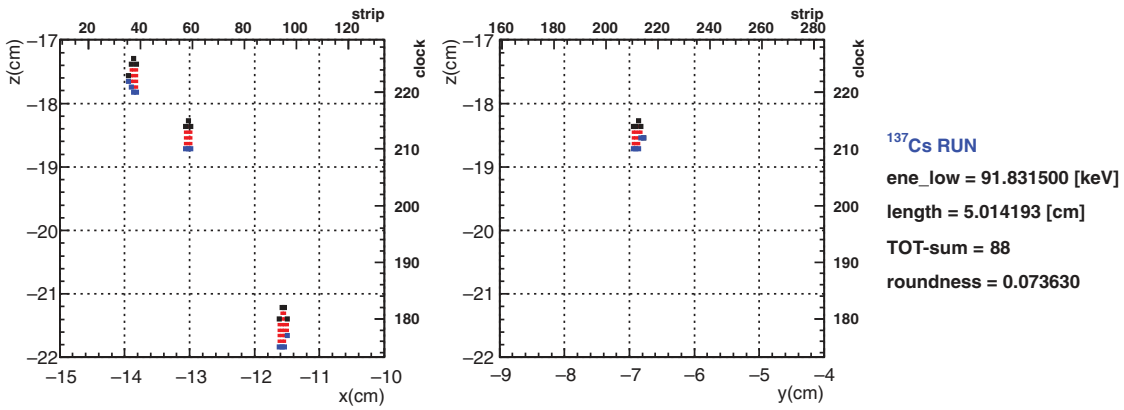

Fig. 4. Track sample from a ^{137}Cs source, cut by the length cut.

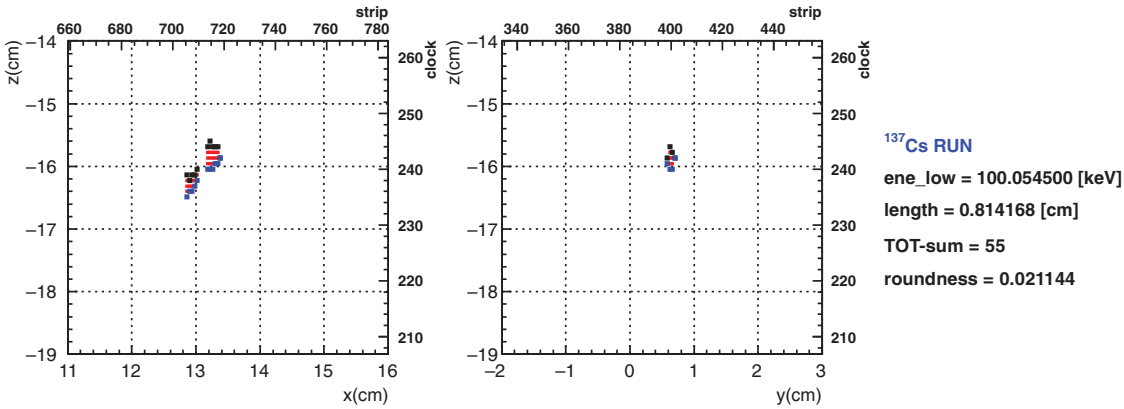

Fig. 5. Track sample from a ^{137}Cs source, cut by the TOT-sum cut.

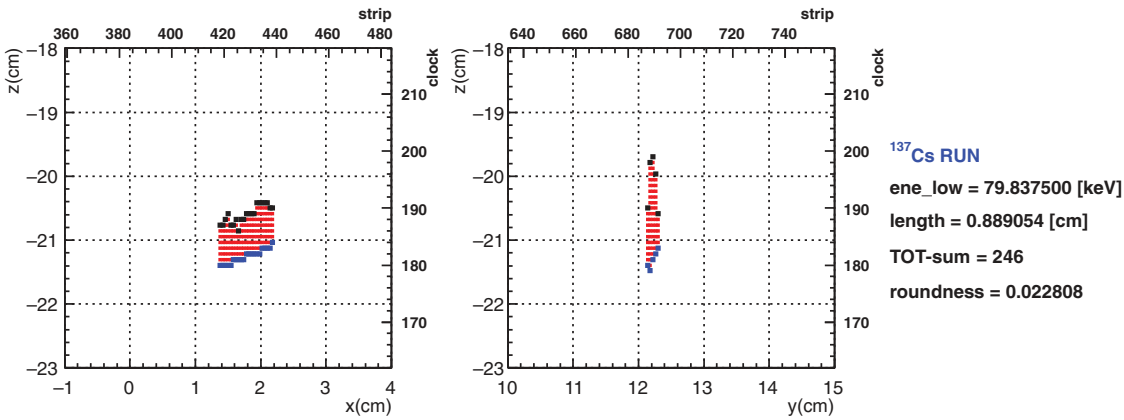

Fig. 6. Track sample of α particle background from μ-PIC, contaminating a ^{137}Cs run. This type of event is cut by the roundness cut.

This cut rejects excessively long track events (see Fig. 4).

- **TOT-sum cut**: TOT-sum < 50.
  This cut rejects non-continuous track events (see Fig. 5).
- **roundness cut**: roundness < 0.05.
  This cut rejects events remaining in the ^{137}Cs run shown in Fig. 9 (see Fig. 6).

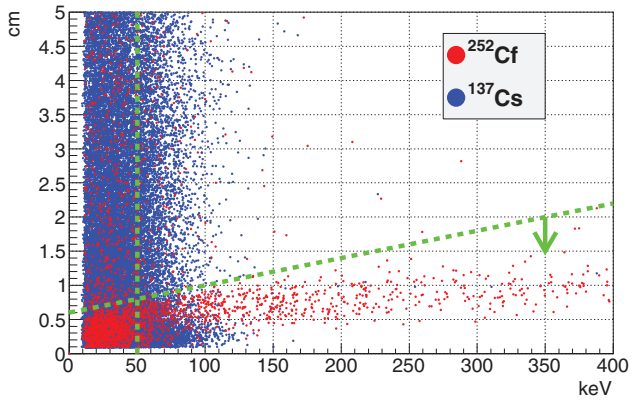

Fig. 7. Dependence of the track length on particle energy. Red and blue points indicate the measured data emitted by a ^{252}Cf source and a ^{137}Cs source, respectively.

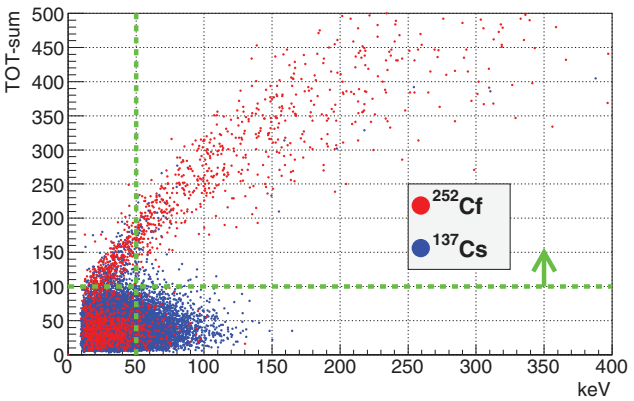

Fig. 8. Dependence of the TOT-sum on particle energy after the length cut. Red and blue points are as described above.

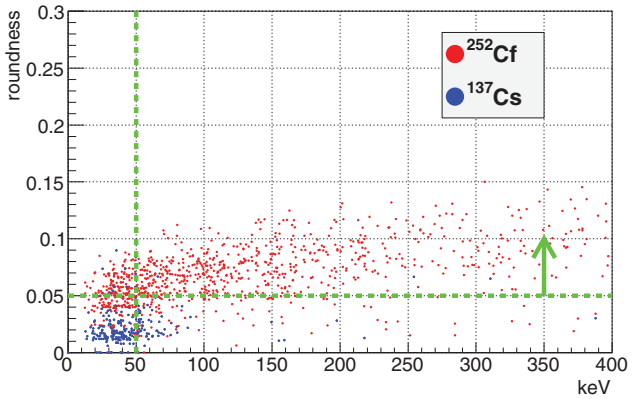

Fig. 9. Dependence of the roundness on particle energy after the length cut and the TOT-sum cut. Red and blue points are as described above.

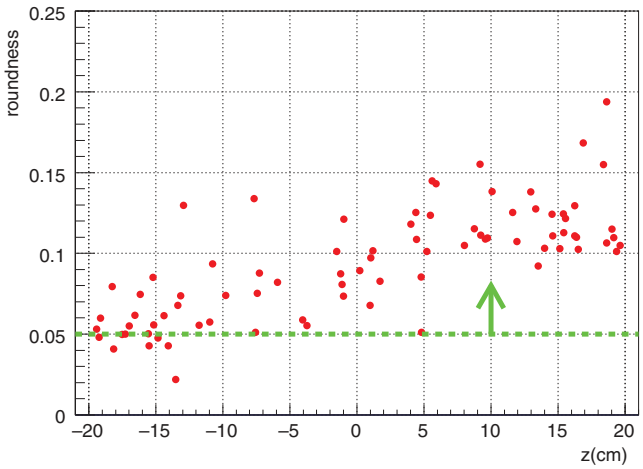

Fig. 10. Measured roundness as a function of the drift length.

The nuclear events shown in Fig. 3 survived all three of these cuts. These cuts effectively reduce the events of a ^{137}Cs run without unduly compromising the efficiency[1] of nuclear track detection (see Figs. 7–9).

In addition, to study the effect of the roundness cut, we irradiated the detector with neutrons from a ^{252}Cf source, and measured the roundness of nuclear events as a function of the drift length. In this measurement, prompt gamma-rays from ^{252}Cf were used as the trigger so as to enable the detection of the absolute z-position of each event. The relation between roundness and drift length is plotted in Fig. 10. The roundness cut is observed to operate as a kind of "z-fiducial cut."

2.4. Performance

Here we discuss the nuclear detection efficiency, electron detection efficiency (or gamma-ray rejection power), direction-dependent efficiency, and the angular resolution.

When measuring the detection efficiency of the nuclear events and the rejection power of the gamma-ray events, we imposed the three cuts introduced in Sect. 2.3. The measured detection efficiency of the nuclear recoil events is shown in Fig. 11. The efficiency is evaluated by dividing the measured energy spectrum after the three cuts explained in Sect. 2.3 by the simulated energy spectrum. The denominator is the simulated energy spectrum of nuclear recoils by the neutrons wiithout the detector response. Thus the estimated efficiency includes the detection and cut efficiency. To cancel the positional dependence, the spectrum was measured at six positions of ^{252}Cf and averaged. The source positions were $(25.5, 0, 0)$, $(-25.5, 0, 0)$, $(0, 25.5, 0)$, $(0, -25.5, 0)$, $(0, 0, 47.5)$, and $(0, 0, -47.5)$. Some bins in Fig. 11 have error bars exceeding 1, because the statistical errors are large in the high-energy region due to the low event rate. We limited the fit parameters so that the efficiency curve shown by the blue line in Fig. 11 does not exceed one, which is a physical requirement. We used this efficiency curve in the following analysis. The detection and cut efficiency is 40% at the 50 keV threshold.

The thresholds of digital signals and cut efficiency decrease the detection efficiency in the low-energy range.

[1] The efficiency measurement is described in the following subsections.

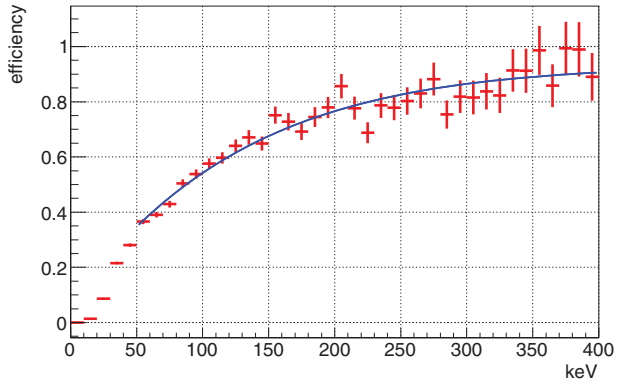

Fig. 11. Detection efficiency of nuclear events as a function of energy. The error bars are statistical ones.

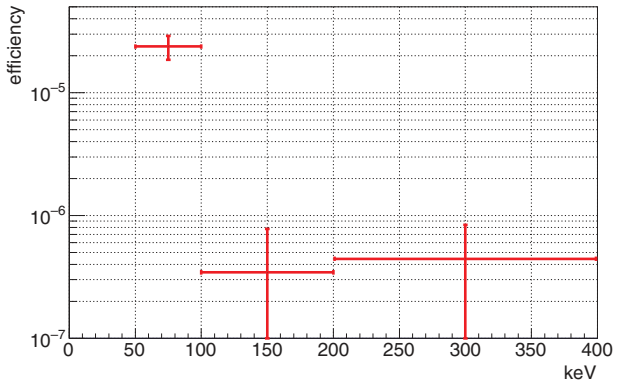

Fig. 12. Detection efficiency of electron events, or gamma-ray rejection power, as a function of energy.

To determine the detection efficiency of electron events, the detector was irradiated with gamma-rays from a ^{137}Cs source and the data were compared with simulated results. Within a given energy bin, the detection efficiency is the measured event rate divided by the simulated event rate of electrons with the same energy. The electron detection efficiency in the energy bin 50–100 keV was evaluated as 2.5×10^{-5}. The electron detection efficiency is plotted as a function of energy in Figure 12.

The direction-dependent efficiency in the 50–100 keV range was measured by irradiating the detector with neutrons from a ^{252}Cf source placed at various positions; namely, at $(25.5, 0, 0)$, $(-25.5, 0, 0)$, $(0, 25.5, 0)$, $(0, -25.5, 0)$, $(0, 0, 47.5)$, and $(0, 0, -47.5)$. For simulations, we confirmed that the weighted average of these six measurements (standard deviation = 23%) properly captures isotropic recoil. In the expected direction distribution of the recoil nuclear tracks scattered by dark matter, the weighting factor is the measured direction-dependent efficiency.

The angular resolution was evaluated from the neutron–nuclei elastic scatterings. Specifically, the measured $|\cos\theta|$ distributions were compared to the simulated distributions, where θ is the angle between the directions of the scattered nuclei and the ^{252}Cf neutron source. In our previous detector study, we measured the angular resolution as 40° at the energy threshold of 50 keV [9].

3. Experiment

A direction-sensitive dark matter search experiment (RUN14) was performed in an underground laboratory at Kamioka mine. NEWAGE-0.3b' was installed in Laboratory B, Kamioka Observatory (36°25′N, 137°18′E), at a depth of 2700 m water equivalent (w.e.). To enable easy access, the detector

Table 2. Summary of RUN14 measurements.

RUN ID	gas filling	DM measurement	live time	mass	exposure
RUN14-1	2013/07/17	2013/7/20–8/11	17.1 days	10.36 g	0.177 kg · days
RUN14-2	2013/10/17	2013/10/19–11/12	14.5 days	10.36 g	0.150 kg · days
RUN14			31.6 days		0.327 kg · days

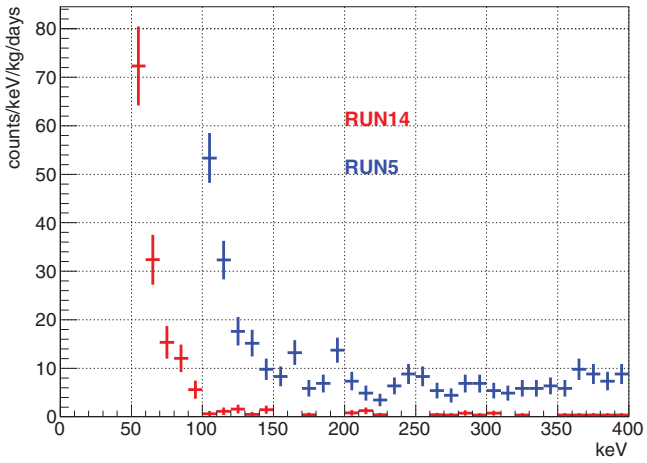

Fig. 13. Energy spectrum acquired in Kamioka RUN14 (red points). Blue points are the results of previous measurements in RUN5 [5,10]. The results are corrected for detection efficiency.

was not surrounded by any radiation shield. The μ-PIC plane of the μ-TPC was vertically positioned and the z-axis was aligned in the direction of S30°E. The run properties are summarized in Table 2. The first sub-run was started by gas filling on July 17, and dark matter measurements continued from July 20 to August 11, collecting an exposure of 17.1 days. The second sub-run started on October 17 and accumulated data from October 19 to November 12, a dark matter exposure of 14.5 days. The target gas was CF_4 at 0.1 atm in a fiducial volume of 27552 cm^3. Thus, the exposure during the first and second sub-runs was 0.177 kg · days and 0.150 kg · days, respectively, giving a total exposure of 0.327 kg · days.

The measured energy spectrum is shown in Fig. 13. The results of our previous run are also shown for comparison. Plotted are the "effective" spectra, corrected for the detection efficiency. Because the angular resolution was measured down to 50 keV, we plotted the energy spectrum of RUN14 from 50 keV. The background rate of RUN14 was $\sim 1/10$ lower than that of RUN5 within the energy range 100–400 keV. The track direction plots and their corresponding $|\cos\theta_{\rm cygnus}|$ distributions in the 50–400 keV energy range are shown in Figs. 14 and 15, respectively. Here, $|\theta_{\rm cygnus}|$ is the angle between the WIMP-wind direction and the measured direction of the recoil nucleus. In dark matter observations, we expect a strong signal from the Cygnus direction. The obtained direction distribution was roughly isotropic, with some excess around $|\theta_{\rm cygnus}| = 0$ and 1. This result may be attributed to the dominant background generated by the detector components, whose spatial distribution is anisotropic. A precise identification of the background source from the directional information is ongoing and will be reported elsewhere (K. Nakamura et al., in preparation). In this paper, we adopt the "conventional" direction-sensitive analysis carried out in our previous works.

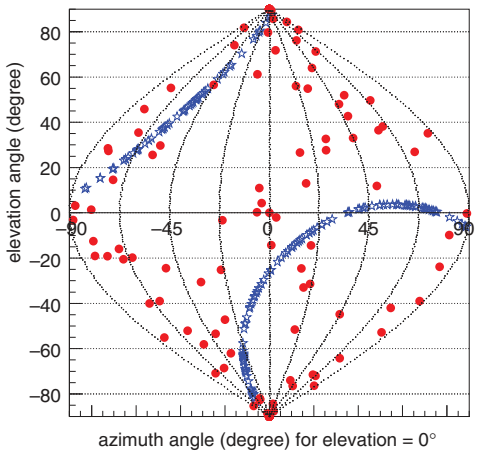

Fig. 14. The directions of nuclear tracks obtained in RUN14 in the 50–400 keV energy range drawn by sinusoidal projection (red). Blue points are the Cygnus direction corresponding to each event. Note that because this analysis does not use head–tail recognition, the range of azimuth angle is up to ±90°.

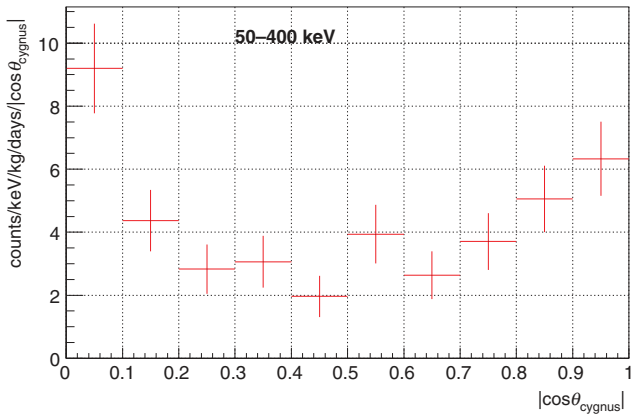

Fig. 15. $|\cos\theta_{\rm cygnus}|$ distribution obtained in RUN14 in the 50–400 keV energy range.

Table 3. Astrophysical parameters, nuclear parameters, and detector responses used to derive the WIMP-proton limits.

WIMP velocity distribution	Maxwellian
Maxwellian velocity dispersion	$v_0 = 220\,{\rm km\,s^{-1}}$
Escape velocity	$v_{\rm esc} = 650\,{\rm km\,s^{-1}}$
Local halo density	$\rho_{\rm DM} = 0.3\,{\rm GeV}/c^2\,{\rm cm^{-3}}$
Spin factor of ^{19}F	$\lambda^2 J(J+1) = 0.647$
Energy resolution at 50 keV	7.8 keV
Angular resolution at 50–100 keV	40°

4. Result

We derived the SD cross-section $\sigma^{\rm SD}_{\chi-{\rm p}}$ limits by the direction-sensitive method, in which the measured $|\cos\theta_{\rm cygnus}|$ distribution was compared with a calculated "expected spectrum." This calculation involved the astrophysical parameters, nuclear parameters, and detector responses listed in Table 3. When the energy range to be used for the analysis is low, it is necessary to take account of the effect of

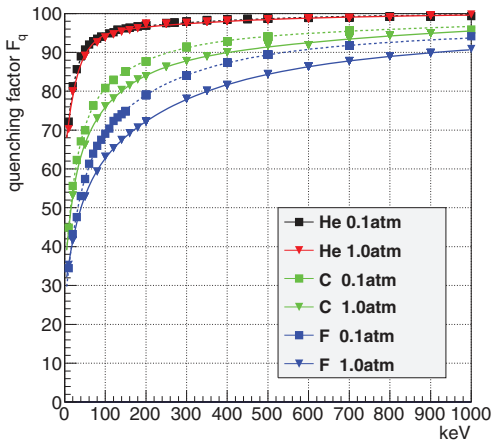

Fig. 16. Quenching factor of various nuclei in CF_4 gas calculated by SRIM [11]. Each line shows different nuclei–pressure combinations, as shown in the legend.

nuclear quenching. The energy is corrected using an ionization quenching factor for 0.1 atm of CF_4 gas simulated by SRIM [11] as shown in Fig. 16. The ionization quenching factor has been measured by the MIMAC group [12], and is greater than the value of SRIM. In order to give a conservative limit in this analysis, we adopted the calculation results of SRIM. To obtain conservative limits, the expected and measured $|\cos\theta_{\rm cygnus}|$ distributions were compared assuming that all measured events are dark matter events. Because of the low statistics, the measured and calculated $|\cos\theta_{\rm cygnus}|$ distributions in every 10 keV bin in the range 50–400 keV were rebinned into two bins and compared with each other. Details of the procedure are provided in [5].

Figure 17 plots the limits of the SD cross-section, $\sigma^{\rm SD}_{\chi-{\rm p}}$, as a function of WIMP mass M_χ. The regions above the curves are excluded at the 90% C.L. The solid red line plots the result of the present work. Our current measurements were also analyzed by the conventional method (spectrum-only) for reference. The two methods give similar results on account of the small statistics. The largest systematic error is the uncertainty in the energy resolution. As described in Sect. 2.2, the energy resolution is determined by $\sigma_{\rm uni} = 20\% \pm 5\%$ and $\sigma_{\rm noise} = 2$ keV. To ensure conservative limits, we assumed $\sigma_{\rm uni} = 15\%$ in the analysis (giving a total energy resolution of 7.8 keV at 50 keV). Figure 18 shows the calculated χ^2/d.o.f. values with the WIMP model (red), and calculated with the flat-background model (black). Because background study is required for a detailed discussion of $\cos\theta$, the data is compared with the isotropic background in this paper. The minimum χ^2 values for less than 70 GeV are shown. As for the 100–1000 GeV mass region, we evaluated the 90% C.L. upper limit by increasing the cross-section until χ^2 values exceeded 2.7. We obtained a 90% C.L. SD WIMP-proton cross-section upper limit of 557 pb for a WIMP mass of 200 GeV. This result marked a new best sensitivity record for an SD WIMP search with the direction-sensitive method, although its sensitivity is still worse than that of the frontier of SD WIMP searches with other methods. The 90% C.L. SD WIMP-proton cross-section upper limit was then obtained as 557 pb for a WIMP mass of 200 GeV. This result is the best sensitivity obtained by the direction-sensitive method in an SD WIMP search, but remains inferior to the frontiers of SD WIMP searches by other methods.

The dominant background radiation of RUN14 was identified as α particles from U/Th-chain contamination in the μ-PIC. This issue will be discussed in detail elsewhere (K. Nakamura et al.,

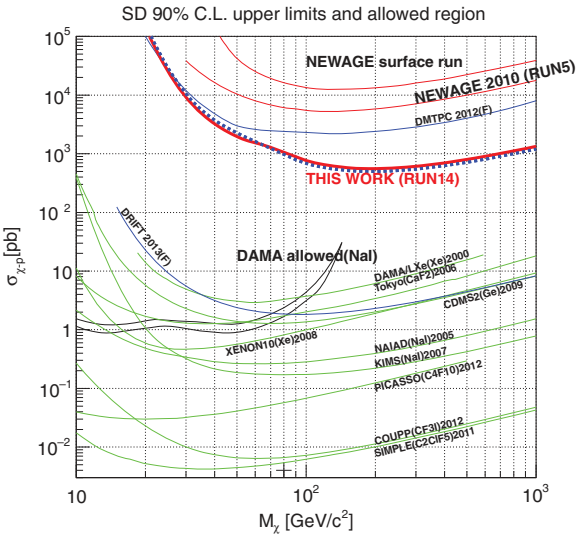

Fig. 17. Limits of SD cross-section, $\sigma^{\mathrm{SD}}_{\chi-\mathrm{p}}$, as a function of WIMP mass M_χ. The thick solid red line plots the result of the present directional method. The results of the conventional method (thick dotted blue line) are plotted as a reference. The thin red lines labeled "NEWAGE surface run" and "NEWAGE 2010 (RUN5)" are previous results measured at the surface and Kamioka, respectively [10]. The allowed region (DAMA [13]) and the upper limits of other experiments are shown for comparison. The solid green and blue lines are the non-directional limits imposed by liquid or solid detectors in conventional analysis (DAMA/LXe [14], NAIAD [15], KIMS [16], Tokyo(CaF2) [17], XENON10 [18], CDMS2(Ge) [19], PICASSO [20], COUPP [21], SIMPLE [22]) and the limits set by gaseous detectors (DM-TPC [23], DRIFT [24]), respectively.

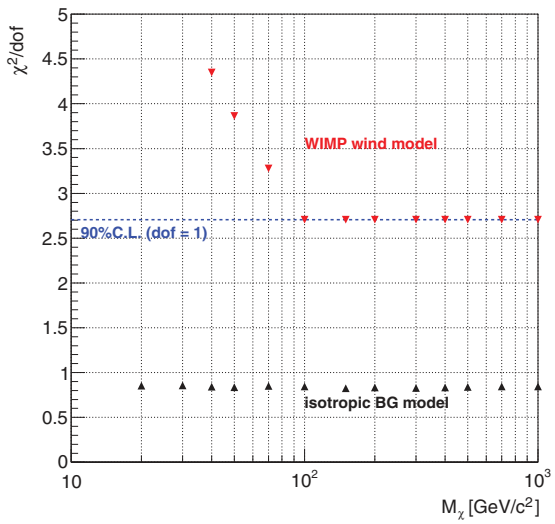

Fig. 18. χ^2 values in comparison with measured $|\cos\theta_{\mathrm{cygnus}}|$ and those of models. Red points are χ^2 values with the WIMP-wind model. Black points are the minimum χ^2 values with the isotropic background model.

in preparation). We have begun developing a new μ-PIC with low background radiation and are planning initial investigations of the DAMA region within the next few years.

5. Conclusion

NEWAGE-0.3b' was employed in a direction-sensitive dark matter search in the Kamioka underground laboratory, undertaken from July 17, 2013 to November 12, 2013. The exposure was evaluated

as 0.327 kg · days, and the 90% C.L. direction-sensitive SD cross-section limit was newly obtained as 557 pb for WIMP masses of 200 GeV/c^2. Compared to our previous measurement, the SD cross-section limits were improved by a factor of ∼10. To date, this is the best direction-sensitive limit achieved by our group.

Acknowledgements

This work was partially supported by KAKENHI Grant-in-Aids (19684005, 23684014, and 26104005); KAKENHI Grant-in-Aids for JSPS Research Fellow.

References

[1] P. A. R. Ade et al., Astron. Astrophys. **571**, A16 (2014).
[2] G. Jungman et al., Phys. Rep. **267**, 195 (1996).
[3] J. D. Lewin and P. F. Smith, Astropart. Phys. **6**, 87 (1996).
[4] D. N. Spergel, Phys. Rev. D **37**, 1353 (1988).
[5] K. Miuchi et al., Phys. Lett. B **686**, 11 (2010).
[6] A. Takada et al., Nucl. Instr. Meth. Phys. Res. Sect. A **573**, 195 (2007).
[7] F. Sauli and A. Sharma, Annu. Rev. Nucl. Part. Sci. **49**, 341 (1999).
[8] H. Kubo et al., IEEE Nucl. Sci. Symp. Conf. Rec. **1**, 371 (2005).
[9] K. Nakamura et al., JINST **7**, C02023 (2011).
[10] H. Nishimura, PhD thesis, Kyoto University (2009).
[11] J. F. Ziegler, J. P. Biersack, and U. Littmark, *The Stopping and Range of Ions in Matter*, (Pergamon Press, Oxford, 1985).
[12] MIMAC, EAS publication series, Proc. CYGNUS 2011, Third Inter. Conf. on Directional Detection of Dark Matter, **53**, 25 (2012).
[13] C. Savage et al., Phys. Rev. D **70**, 123513 (2004).
[14] R. Bernabei et al., New J. Phys. **2**, 15.1 (2000).
[15] G. J. Alner et al., Phys. Lett. B **616**, 17 (2005).
[16] H. S. Lee, et al. (KIMS Collaboration), Phys. Rev. Lett. **99**, 091301 (2007).
[17] Y. Shimizu et al., Phys. Lett. B **633**, 195 (2006).
[18] J. Angle, et al. (XENON Collaboration), Phys. Rev. Lett. **101**, 091301 (2008).
[19] Z. Ahmed et al. (CDMS Collaboration), Phys. Rev. lett. **102**, 011301 (2009).
[20] S. Archambault et al., Phys. Lett. B **711**, 153 (2012).
[21] E. Behnke et al., Phys. Rev. D **86**, 052001 (2012).
[22] M. Felizardo et al., [arXiv:1106.3014v3] .
[23] S. Ahlen et al., Phys. Lett. B **695**, 124 (2011).
[24] E. Daw et al., Astropart. Phys. **35**, 397 (2012).